

Revealing the Influence of Electrolyte Additives in Reducing the Heat Generation of High Voltage Lithium-Ion Batteries using Operando Accelerating Rate Calorimetry (ARC)

Mariam Baazizi,^[a, b] Simon Sayah,^[b] Mehdi Karbak,^[b, c] Oumaima Hajjaj,^[b] Mohamed Aqil,^[a] Mouad Dahbi,^[a] and Fouad Ghamouss^{*[a, b]}

Lithium-ion batteries operating at high voltage generally endure drastic capacity fading and serious safety issues. Working on the electrolytes' stability can be a solution to mitigate these problems related to high voltage. Herein, the beneficial impact of functional electrolyte additives in a state-of-the-art carbonate-based electrolyte is demonstrated. The combination of fluoroethylene carbonate (FEC) with succinonitrile (SN) as additives was used to enhance the thermal stability of the electrolyte reference 1 M LiPF₆ in EC:DMC (1:1, by weight) and cycling stability of a high voltage lithium-ion device, consisting of a LiMn_{1.5}Ni_{0.5}O₄ cathode and a metallic lithium anode. The electrolyte using the FEC/SN mixture displayed a wider electro-

chemical stability window (ESW) exhibited by linear sweep voltammetry (LSV). Furthermore, this electrolyte allowed the device to exhibit better rate capability and a capacity retention of 75% after 100 cycles. Interestingly, the FEC+SN-based electrolyte exhibited better thermal stability using operando accelerating rate calorimetry (ARC) by virtue of the lower heat quantity generated by the battery device. The remarkable improvements can be ascribed to the formation of a protective cathode-electrolyte interface (CEI) produced by interfacial reactions between the cathode surface and electrolyte compounds.

Introduction

The growing public concern over the environment, energy, and sustainable development has made the improvement of next-generation energy storage technologies with high energy and power densities and environmentally friendly benefits a pressing priority.^[1] High-voltage lithium-ion batteries (LIBs) have emerged as a promising solution for increasing energy and provided power density.^[2] This is achieved through the use of high-voltage cathode materials that can reach potentials of 5 V or higher.^[3–6] For instance, electrodes like lithium nickel manganese cobalt oxide (NMC)^[7,8] or lithium manganese nickel oxide (LMNO)^[9–11] can both achieve high-voltage, thus, deliver-

ing high energy and power densities. However, these systems suffer from serious safety issues by virtue of the structural degradation, transition metals dissolution, electrolytes high flammability or irreversible side reactions, etc.^[12,13]

To date, several approaches have been used to improve the electrochemical stability of high voltage cathode materials including surface modifications^[2,14–16] and metal doping.^[17–20] However, the modification of electrode materials involves higher cost and complicated processes to be implemented in the industrial scale. Since stable electrolytes with high interface compatibilities can hinder these limitations, controlling their composition is an efficient strategy to develop balanced high-voltage electrolytes.^[21] Consequently, developing novel stable solvents and finding new multifunctional additives have been the target of various research scientists. Ionic liquids,^[22–24] sulfone^[25] or nitrile^[26,27] compounds and fluorinated solvents^[28–30] are examples of the commonly investigated solvents or cosolvents. In addition, the incorporation of various additives into conventional electrolytes to alter the cathode-electrolyte interface (CEI) has garnered significant attention in the field of high voltage LIBs to improve their performance. Precise examples are film-forming additives in electrolyte such as fluorinated and dinitrile based compounds, namely fluoroethylene carbonate (FEC)^[11–15] and succinonitrile (SN).^[36–39]

FEC and SN have been shown to improve the electrode-electrolyte interface compatibility. This is achieved through the formation of a protective layer on the electrode's surface, created from the electrochemical decomposition products of these additives and occurring at lower potentials than carbo-

[a] M. Baazizi, M. Aqil, M. Dahbi, F. Ghamouss
Materials Science,
Energy, and Nano-Engineering department
Mohamed VI Polytechnic University
Ben Guerir (Morocco)
E-mail: fouad.ghamouss@um6p.ma

[b] M. Baazizi, S. Sayah, M. Karbak, O. Hajjaj, F. Ghamouss
Laboratory of Physical-Chemistry of
Materials and Electrolytes for Energy (PCM2E)
University of Tours
37200 Tours (France)

[c] M. Karbak
Laboratory of Chemical Engineering and
Resources Valorization (LGCVR)
University Abdelmalek Essaadi
B.P. 416, Tangier 90010 (Morocco)

 Supporting information for this article is available on the WWW under
<https://doi.org/10.1002/batt.202300151>

nates decomposition, thereby improving the overall stability of the battery.

The high electronegativity and low polarity of fluorine atoms make fluorinated organic solvents highly beneficial to high-voltage electrolytes. As previously reported, FEC can readily degrade and form an inorganic LiF-rich CEI protective film on the surface of electrodes. It undergoes decomposition before the electrolyte itself, acting as a sacrificial component to create a protective layer CEI. This addition of FEC not only suppresses the decomposition of the electrolyte but also promotes the formation of a more conductive passivation film on the cathode's surface. This conductive film facilitates the migration of Li^+ ions into the cathode material and shields the electrode surface from corrosion and unwanted interactions with the electrolyte.^[40] Park et al. reported a remarkable improvement of the cycling stability and electrode-electrode interface resistance of the LiCoO_2 cathode material at 4.5 V after adding 1.0 wt% FEC to the conventional electrolyte.^[41] Liu et al. used 5.0% FEC as additive and improved the cycling stability of a LiCoO_2 graphite full cell at 4.4 V.^[42] Moreover, 2.0% FEC was able to improve the electrochemical performance of a 5 V $\text{LiNi}_{0.5}\text{Mn}_{1.5}\text{O}_4$ cathode material to a capacity retention of 96.2% after 150 cycles, as reported by Xu et al.^[43] Furthermore, FEC was studied as solvent and co-solvent for high voltage electrolytes and presented excellent results.^[28,29,44–46] As an example, replacing EC with FEC in a $\text{LiNi}_{1/3}\text{Co}_{1/3}\text{Mn}_{1/3}\text{O}_2$ battery could double the capacity retention to 82.7% after 100 cycles at 4.6 V.^[46] Hence, FEC was found to be highly effective both as a high-voltage additive and solvent in LIBs.

SN is also considered as an ideal organic solvent by virtue of its high oxidation tolerance and excellent thermal stability. Consequently, it has been widely studied as a plasticizer or additive in liquid electrolytes and polymer based solid-state electrolytes.^[47–49] SN additives improve the Li^+ conductivity and broadens the electrochemical stability window (ESW). Moreover, as an additive, SN can stabilize LiPF_6 salt by eliminating trace water in the electrolyte and hydrolyzing the erosive hydrofluoric acid (HF), thus alleviating the metal ions dissolution phenomena on the positive electrode surface.^[26,39] Based on DFT calculations, Zhi et al. investigated the mechanism of the SN electrolytes surface stabilization at high voltages. They suggested that the formation of a cathode interface originates from the oxidative decomposition of nitriles on the cathode surface and refuted the previously-established theory that the chemisorption of SN on the cathode surface inhibits the electrolyte decomposition. In fact, the interaction of SN with salt anion reduces its oxidation resistance and hence easily form a N-containing interphase (Li_3N and LiN_xO_y) prior to carbonates decomposition.^[26,38]

Even though the scientific interest was fairly focused on FEC and SN as additives for LIBs, not enough studies investigated the thermal stability of devices either with or without these functional additives. The ability of a battery to maintain consistent and safe operation when exposed to varying temperatures is referred to as thermal stability. It is a crucial parameter that is indicative of its cycling performance. During the charge-discharge cycles, heat is generated due to the internal electro-

chemical reactions that take place in the battery. The failure to dissipate this heat efficiently can lead to the degradation of the electrodes, electrolyte, and other components of the battery. This can result in a decline in performance and capacity, as well as an increase in the risk of failure. By evaluating the thermal stability of a battery, researchers can obtain a better understanding of its performance under varying operating conditions. Furthermore, thermal stability testing can also provide information on the kinetics of the electrochemical reactions that take place in a battery system, which can aid in the development of new materials, electrolyte formulations and designs.

Motivated by previous reports, different electrolyte systems (additive free, FEC, SN and SN+ FEC) has been prepared to investigate the electrochemical performance of the $\text{LiMn}_{1.5}\text{Ni}_{0.5}\text{O}_4$ cathode under high-voltage conditions. In addition, we studied, for the first time to our knowledge, the effect of the combination of these electrolyte additives on the electrochemical performance of the high voltage $\text{LiMn}_{1.5}\text{Ni}_{0.5}\text{O}_4/\text{Li}$ system. Furthermore, physical characterizations and electrochemical measurements were carried out to analyze the electrode-electrolyte interface (CEI) and cycling stability. Finally, operando accelerating rate calorimetry (ARC) tests were conducted to evaluate the thermal behavior and quantify the heat emitted by batteries using different electrolytes with and without additives in the high voltage $\text{LiMn}_{1.5}\text{Ni}_{0.5}\text{O}_4/\text{Li}$ system.

Results and Discussion

To evaluate the potential impact of our additives on the electrochemical and thermal performance of electrolytes in lithium-ion batteries, some of their physical and transport properties have been determined, specifically their density, viscosity, ionic conductivity, and thermal behavior via differential scanning calorimetry (DSC) analysis. Indeed, low density/viscosity and high ionic conductivity would be desirable. Additionally, electrolytes should exhibit high thermal stability, as indicated by high degradation temperatures and low heat generation, to ensure safety.

Figure 1(a) shows the variation of the density of each prepared electrolyte as a function of temperature from 283 to 353 K with an uncertainty lower than $5.00 \times 10^{-5} \text{ g cm}^{-3}$. The temperature T increase causes a perfectly linear decrease in the density ρ . Equation (1) is a result of the linear fitting of the density curve ($R^2 = 1.00$) for all electrolytes.

$$\rho = a - bT \quad (1)$$

In fact, the density represents the salt-electrolyte interactions. The temperature basically decreases the strength of intermolecular interactions, therefore, the decrease of the densities. In other words, the number of ions per unit volume reduces with temperature. At 25 °C, studied electrolytes presented densities of 1.295, 1.285, 1.285, and 1.272 g cm^{-3} respectively for the additive free, FEC, FEC+SN and SN. All these densities are in line with the density of commercialized electrolyte (additive free) as they are around 1.30 g cm^{-3} .

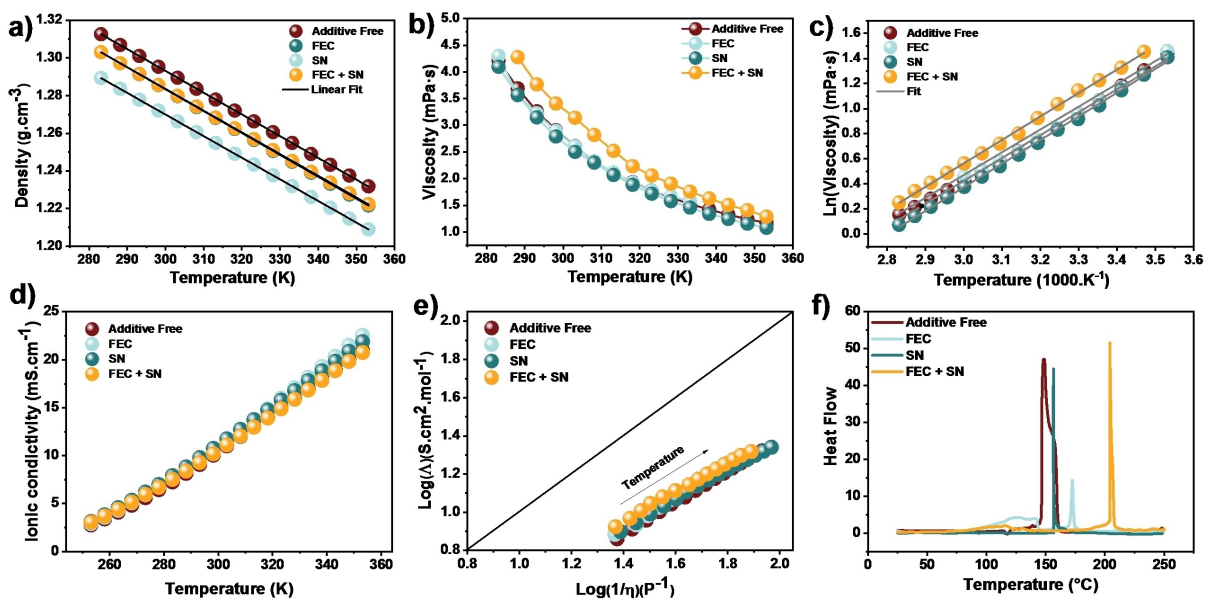


Figure 1. a) Density values linear fitted between 283 and 353 K, b) viscosity measurements between 283 and 353 K, c) Arrhenius plot of the viscosity, d) ionic conductivity from 253 to 353 K, e) Walden product data, f) DSC curves between –60 and 250 °C for the additive free electrolyte, FEC, SN and FEC + SN.

Temperature dependence of the electrolytes viscosities was also studied over the temperature range 283–353 K (figure 1.b). It can be seen from the graph that the viscosity decreases with increasing temperature. In addition, at high temperatures (353 K) the viscosities values are closer compared to the ambient temperature (298 K) where the difference is more important. As at high temperatures, particles move faster, undergo shorter interactions and reduced internal stress and friction. The figure also revealed that the addition of 2 additives (FEC + SN) resulted in an increase in the viscosity compared to the additive free and 1 additive electrolytes by virtue of the increased molecular weight.

All plots were fitted with the logarithmic form of the Arrhenius (Eq. 2) (Figure 1c).

$$\ln \eta = \ln \eta_{\infty} + E_{\eta} / RT \quad (2)$$

where, R is the gas constant ($8.314 \text{ J mol}^{-1} \text{ K}^{-1}$) and T temperature in K. The viscosity at infinite temperature (η_{∞}) and the activation energy for viscous flow (E_{η}) are calculated respectively from the intercept and the slope of the Arrhenius plot and presented in Table 1. E_{η} is the energy barrier which must be overcome by the ions in motion. The value of this activation energy (E_{η}) can be correlated with the structural properties of our electrolytes. At infinite temperature, interactions that normally contribute to viscosity at ambient temperature are no

longer effective and the viscosity η_{∞} is mainly controlled by the geometric structure of the ions. Therefore, η_{∞} is representative of the structural contribution of the ions to the viscosity.

The ionic conductivities of studied electrolytes with selected additives were investigated between –20 and 80 °C (Figure 1d). The ionic conductivities increased expectedly with increasing temperature as demonstrated by the Arrhenius law. At 25 °C, the ionic conductivities of the additive free electrolyte, FEC, SN and SN + FEC are 10.04, 10.60, 10.75 and 10.18 mS cm⁻¹ respectively (Table 2). The addition of one additive (SN or FEC) slightly increased the ionic conductivity, however the addition of two additives (SN + FEC) affected it negligibly. This might be originated from the increased viscosity of the SN + FEC electrolyte.

To evaluate the dissociation abilities of electrolytes solvents, we calculated their Walden Products [Equation (3)]. The latter correlates the molar ionic conductivity (Λ) with the viscosity (η) through a temperature dependent constant (k). This law is often used to evaluate the ionic transport and ionicity of ionic liquids to classify them as superionic or subionic solutions. Figure 1(e) presents a plot of the electrolytes Walden products for temperatures from 10 to 80 °C. The line in the middle is the ideal line for a 0.01 M aqueous KCl solution.

$$\Lambda \eta = k \quad (3)$$

Table 1. Arrhenius viscosity equation parameters for prepared electrolytes.			
Electrolytes	η_{∞}	E_{η} [kJ mol ⁻¹]	R^2
Additive Free	6.39×10^{-3}	15.12	0.9964
FEC	5.47×10^{-3}	15.54	0.9932
SN	5.06×10^{-3}	15.62	0.9988
FEC + SN	6.41×10^{-3}	15.53	0.9986

Table 2. Transport properties of prepared electrolytes at 25 °C.

Electrolytes	Density [g cm ⁻³]	Viscosity [mPa s]	Ionic conductivity [mS cm ⁻¹]
Additive free	1.29	2.90	10.04
FEC	1.28	2.89	10.60
SN	1.27	2.78	10.75
FEC + SN	1.28	3.40	10.18

As a result, all our plots are located below the ideal line of the Walden product regardless of temperature and additive type and therefore present subionic behaviors. In general, the deviations below the ideal line can be originated from dynamics hindering effects including ion-pairing that also reduces the net charge transport. The important deviation of our Walden products from the ideal line is an indicator of ion association. It is worth noting that no considerable difference can be noticed in the electrolytes ionicities.

During the operation of a battery, localized thermal events are a common occurrence. Under certain circumstances, these events may lead to the phenomenon known as thermal runaway, or in severe cases, a battery explosion. To mitigate these risks, it is important to examine the thermostability of the electrolytes used in the battery system. This analysis can provide insight into the behavior of these substances at elevated temperatures, which is crucial for optimizing battery performance in high temperature environments. In Figure 1(f), DSC curves for electrolytes with and without additives are shown. It is evident from all curves that there is a distinct exothermic peak, which may be caused by electrolyte degradation. It can be observed that the onset temperature of the exothermic reaction for the additive-free electrolyte is 139 °C. However, when FEC, SN, and a combination of FEC + SN are added to the electrolyte, the onset temperature is significantly increased to 155 °C, 167 °C, and 190 °C, respectively. These results indicate that the addition of the electrolyte mixture (FEC + SN) significantly enhances the thermal stability of the electrolyte, hence, widening the application range of these battery types.

The electrochemical stability window (ESW) of an electrolyte refers to the range of potentials for which the electrolyte is stable and does not undergo chemical decomposition. The stability of the electrolyte is critical for the performance and lifetime of a lithium-ion battery. If the voltage of the battery exceeds the ESW of the electrolyte, the latter can undergo unwanted chemical reactions that generate byproducts and reduce the overall performance and lifetime of the battery. Therefore, it is important to select an electrolyte with an appropriate ESW for the intended application to ensure that the battery operates reliably and efficiently. It is typically determined by measuring the potential at which the electrolyte decomposes, either through the use of electrochemical techniques or by observing the formation of byproducts during long-term aging tests.

In this work we opted for linear sweep voltammetry (LSV) to highlight the effect of additives on our electrolytes oxidation and reduction stability. In LSV, the potential of the electrolyte is swept linearly over a range of values, and the current flowing through the electrolyte is measured. The potential at which the current begins to increase significantly can be taken as the lower limit of the electrochemical stability window. Figure 2 displays the comparison of obtained results. As shown in Figure 2, the electrolyte without additives containing only the lithium salt and solvents presented the lowest oxidation resistance, with the oxidation peak and electrolyte degradation starting at 2.2 V vs. Ag⁺/Ag (Eq 6.05 V vs. Li⁺/Li). Adding the

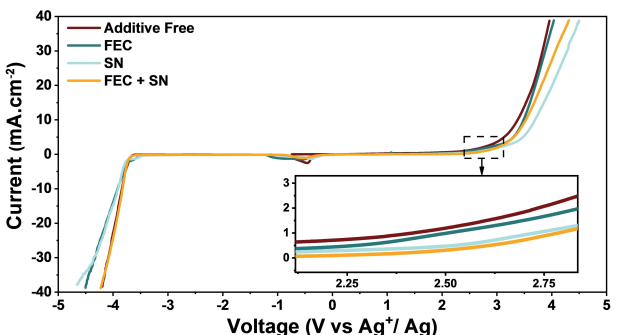


Figure 2. LSV at 5.0 mVs⁻¹ for the additive free electrolyte, FEC, SN and FEC + SN. A silver wire is used as a reference, and platinum as the working and counter electrode. Room temperature.

fluoroethylene carbonate additive (FEC) slightly shifted the oxidation voltage of the electrolyte to a higher voltage 2.3 V vs. Ag⁺/Ag. Moreover, the succinonitrile (SN) additive further broadened the electrochemical stability window to 2.6 V vs. Ag⁺/Ag. The addition of the additives mixture (FEC + SN) to the electrolyte presented the largest electrochemical stability window (2.7 V vs. Ag⁺/Ag) by slightly shifting the oxidation peak to higher voltages compared to the SN alone electrolyte. This finding suggests a synergistic effect of the additives that will be further investigated in the following sections.

To evaluate the effect of the electrolyte additives on the overall electrochemical performance of the battery, different tests were conducted. The galvanostatic charge/discharge (GCD) curves of the Li/LMNO cells using all electrolytes were carried out at 0.1 C between 3.5–5.0 V vs. Li⁺/Li at room temperature. As shown in Figure 3(a), the GCD profiles are very similar with well-defined plateaus and very alike discharge capacities; 126, 125, 125 and 127 mAhg⁻¹ were delivered by the additive free, FEC, SN and FEC + SN systems respectively. This indicates that the electrolyte modification did not affect the electrochemical properties of the material. In addition, the 5th cycle shows capacities that are very close to those obtained in the 1st cycle (128, 130, 127 and 131 mAhg⁻¹ for the additive free, FEC, SN and FEC + SN systems respectively) and reversible for all studied electrolytes (Figure 3b).

The evolution of the discharge capacities versus cycles number of the Li/LMNO half-batteries are presented in Figure 3(c and d). Figure 3(c) shows that the electrolyte with FEC + SN additives has the best rate capability and resistance to current rates change compared to the other electrolytes especially at high rates. It barely shows any specific capacity decrease even at a 1 C rate (135 mAhg⁻¹). On the other hand, the electrolyte with FEC presented the lowest capacity at 1 C delivering around 70 mAhg⁻¹ and retaining only 56% of its initial capacity. Moreover, the electrolytes without additives and with SN were presented around 116 and 109 mAhg⁻¹ respectively. In Figure 3(d) the impact of the various additives on long-term cycling of Li/LMNO devices under a current rate of 0.5 C at 25 °C is very noticeable. Battery cells containing the electrolyte with FEC and SN additives have in addition to their high capacity at different rates, the best capacity retention after

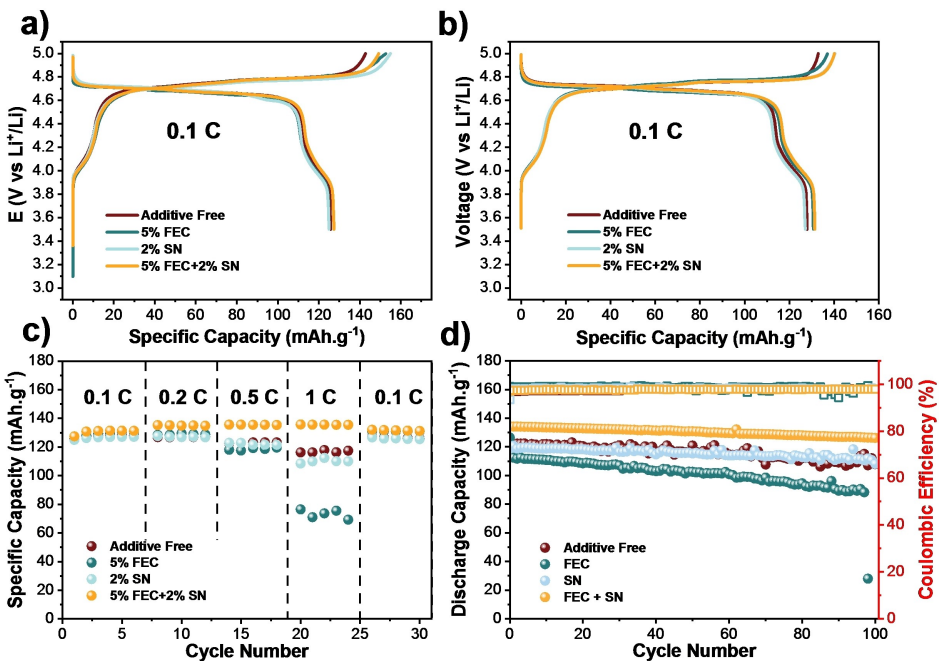


Figure 3. GCD patterns at 0.1 C of a) first cycles, b) fifth cycles c) rate capability, d) long-term cycling at 0.5 C of the additive free, FEC, SN and FEC + SN electrolyte in a Li/LMNO battery cell.

100 cycles. In the presence of FEC alone, the capacity at the first cycle is relatively similar to the cell containing SN alone and the additive free cell. However, capacity losses are much greater with FEC than with SN and the reference electrolyte.

The capacity retention and rate capability results confirm that the FEC+SN mixture improves the electrochemical performance of high voltage cathode materials and confirm that electrolyte development is a key factor to improve the overall stability and capacity of lithium-ion batteries.

To further analyze the improvement of electrochemical properties for the LMNO cathode using the FEC and SN additives, the interfacial property and structural stability of the LMNO cathode before and after 3 cycles at 0.2 C in different electrolyte systems are characterized using scanning electron microscopy (SEM). Compared with the additive free electrolyte in Figure 4, all electrolytes form an inhomogeneous transparent surface layer known as the cathode electrolyte interface (CEI).

Results are shown Figure 4. This passivation layer is the by-product of various reactions between the electrode material and the electrolyte, which make it highly important for high-voltage active material (LMNO). The CEI acts as a protective layer. The performance of the LIB depends on the mobility of lithium ions in both the electrodes and electrolyte, making the CEI significant in high-voltage cathodes (5 V in this work). However, no significant difference was noticed in the particles' morphology between the studied electrolytes. These results indicate that all our studied additives participated in the CEI formation on the cathode surface and hence suppressed parasite reactions between the highly reactive cathode surface and electrolytes. Therefore, the stabilized interface participated

mainly in the betterment of the electrochemical performance of our modified electrolytes.

The EIS spectra provide information about the kinetics of the charge transfer processes and the transport of ions through the electrolyte. The impedance at high frequencies reflects the interfacial charge transfer process, while at low frequencies it is attributed to the ions diffusion. In the EIS spectra, the shape of the curve is typically composed of a semicircle and then a linear region at high and low frequencies respectively. The semicircle represents the charge transfer resistance at the interface between the electrode and the electrolyte, while the linear region stands for the diffusion of ions through the electrolyte.

Therefore, to confirm the interfacial stability of the LMNO in the electrolytes with and without additives, EIS was performed. Figure 5 presents the spectra of pristine LMNO at the OCV and the cycled LMNO after 10, 50 and 100 discharges at 1 C in the voltage window 3.5–5.0 V.

The LMNO in FEC+SN electrolyte has a significantly lower interfacial impedance compared to the other electrolytes all along the 100 cycles. In fact, it exhibited an impedance of around 50, 25 and 25 Ohm cm² after 10, 50 and 100 cycles respectively. These results demonstrate that the combination FEC+SN to the electrolyte improves the cathode electrolyte interface stability (CEI) of the high voltage cathode LMNO. Moreover, the influence of interfacial resistances on the electrochemical behavior, particularly the rate performance, of a material is well-established. In this context, the superior performance of LMNO in a FEC+SN-containing electrolyte compared to the additive free electrolyte can be attributed to the reduced interfacial resistances.

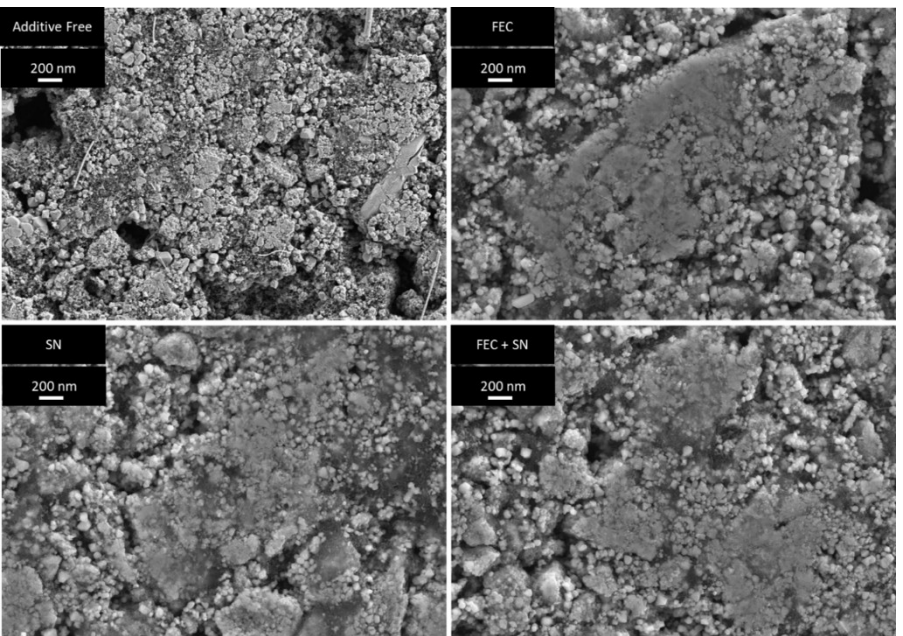


Figure 4. SEM images of the LMNO cathode's interface after 3 cycles at 0.2 C for the additive free, FEC, SN and FEC + SN electrolytes

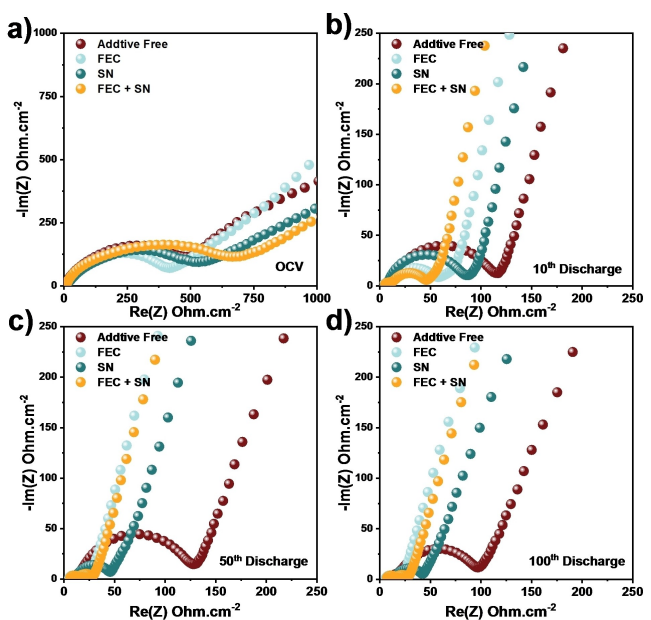


Figure 5. EIS patterns at a) the open circuit voltage, b) 10th discharge, c) 50th discharge, and d) 100th discharge of the Li/LMNO devices with additive free, FEC, SN and FEC + SN electrolytes.

To further understand the role of additives on the overall charge-discharge behavior, it is important to quantify the lithium-ion diffusion into the bulk electrode. This metric helps visualize the tangible performance of additives in a high-voltage battery system. It was already established by Ho et al.^[50] how impedance spectroscopy can be used to identify lithium-ion diffusion (D_{Li^+}) using equation 4.

$$D_{Li^+} = \frac{R^2 T^2}{2\sigma^2 n^4 C^2 F^4 \omega^{1/2}} \quad (4)$$

where R represents the molar gas constant ($8.4145 \text{ J mol}^{-1} \text{ K}^{-1}$), T the temperature in kelvin, F the Faraday's constant (96486 C mol^{-1}), S the electrode's surface in cm^2 , C the Li^+ concentration in bulk electrode (mol cm^{-3}), n is the number of charge carrier and σ can be obtained from the slope of the $\text{Re}(Z)$ vs. $\omega^{-1/2}$, where ω represents the angular frequency in rad s^{-1} .

As shown in Figure 6(a), all assembled systems were plotted [$\text{Re}(Z)$ vs. $\omega^{-1/2}$] at different cycles. Afterward, all slopes were used to calculate D_{Li^+} . As a result, the evolution of the Li^+ diffusion coefficient during cycling was represented in Figure 6(b). At the first cycle, the FEC+SN electrolyte system shows a superior D_{Li^+} next to FEC, SN and additive-free systems (6.81×10^{-14} , 3.10×10^{-14} , 8.64×10^{-15} , $4.64 \times 10^{-15} \text{ cm}^2 \text{s}^{-1}$ respectively). During cycling, the FEC + SN electrolyte keeps a relatively high Li^+ diffusion coefficient next to the other systems, even though the D_{Li^+} coefficient seems unstable. It maintains a $10^{-14} \text{ cm}^2 \text{s}^{-1}$ range. Considering this diffusion kinetics, these results explain the high-rate capability of FEC + SN even at a 1 C current density. In addition, the high diffusion kinetics promotes a better cycling stability even after 100 cycles.

The ex-situ DSC curves in Figure S1 demonstrate the thermal stability of the charged state of LMNO after one charge cycle to 5 V in contact with the additive free and additives containing electrolytes. An exothermic peak was observed for the additive free charged LMNO at approximately 190 °C. However, the onset of the same peak shifted to higher temperatures using modified electrolytes to reach 215, 225 and 230 °C for FEC, SN and FEC+SN electrolytes respectively. This

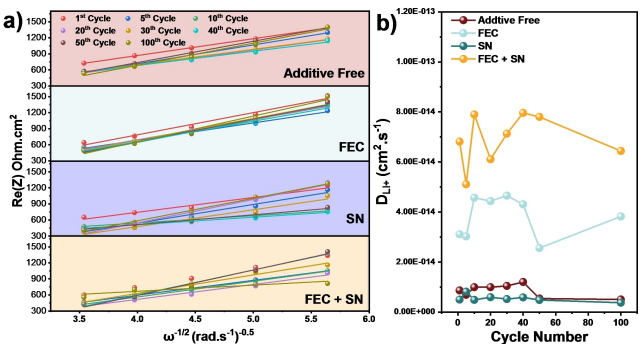


Figure 6. a) The plots of the real part of impedance $\text{Re}(Z)$ as a function of the inverse square root of angular frequency ($\omega^{-1/2}$) at different discharge cycles, b) Lithium diffusion coefficient (D_{Li^+}) as a function of cycles number for the additive free, FEC, SN and FEC + SN electrolytes.

indicates that the differing electrolyte composition has an impact on the decomposition temperature and heat flow of the cathode material at high voltages. This suggestion will be further deepened in the next section dedicated to the in-situ thermal study of the LMNO and electrolytes.

The development of electrolytes is of great importance in optimizing the thermal stability of a lithium-ion battery. The reactions occurring in the cathode-electrolyte interface are exothermic in nature, meaning that they release heat. By understanding the properties of different electrolytes and how they affect the rate and enthalpy of the electrochemical reactions, it is possible to design electrolytes that minimize the amount of heat evolved and enhance the thermal stability of the battery. Operando accelerating rate calorimetry (ARC) is a technique that can be used to investigate the thermal stability of a lithium-ion battery by measuring the heat emitted during electrochemical reactions. In this section, we evaluated the previously defined electrolytes and investigated the heat evolved in the charge-discharge process of the LMNO/Li system between 3.5 and 5.0 V. Hence, we can pinpoint electrolytes that are more thermally stable and can be used to improve the performance and safety of the battery.

Figure S2 presents the results obtained with the additive free electrolyte at a current rate of 1 C for 5 cycles. The current, voltage and heat flux profiles are shown as a function of the acquisition time. It is a convenient way to relate battery charge states to heat flux.

To monitor the system's thermal stability and degradation at a stressed state, a 2-hour floating at the end of charge (5.0 V) was carried out for each cycle.

While charging, the lithium ions are transferred from the cathode to the anode thus increasing the voltage and the heat flux. When the battery reaches 5.0 V, the floating begins. The potential is therefore maintained at 5.0 V without application of current and the heat flux decreases during the 2 hours, which is due to the absence of polarization resistance.^[51] When discharging the battery, the opposite current is applied which decreases the potential to 3.5 V and the heat flux increases again. Note that all heat fluxes are issued from exothermic reactions.

During the following charge/discharge cycles, the heat fluxes evolve in the same way. It starts with an increase when charging the battery, before decreasing during floating at 5.0 V and then increasing again when discharging. The main difference is that the heat flux obtained during the 1st charge is more pronounced than during the next charges. This is due to the formation of the CEI on the surface of the LMNO electrode, consisting of the oxidation products of the species present in the electrolyte and increase of the interfacial resistance. These phenomena mainly take place during the 1st cycle. This modification of the electrode/electrolyte interface greatly reduces oxidation in subsequent cycles, which significantly reduces the generation of internal heat. The heat flux is much greater when discharged. This was found to be remarkably correlated with the internal resistance of LIBs. In fact, when discharging, the battery polarization and the internal resistance get extreme leading to the increase of the irreversible heat inside the battery.^[52,53]

To efficiently investigate the thermal behavior of each electrolyte system in a LIB cell, it is crucial to choose a current density in which the generated heat flux is purely faradaic and doesn't involve any resistive Joule effect. Therefore, the effect of current rates on a LMNO/Li half-cell was studied at 1.0 C, 1.5 C, 2.0 C, 2.5 C, 3.0 C and 4.0 C with a floating of the upper (5.0 V) and low (3.5 V) voltage of 2 h for each cycle under a temperature of 35°C. The current, voltage and heat flux profiles for each C-rate are presented in Figure 7. The electrolyte used in this study is the additive free electrolyte. The heat generation ($\mu\text{Wh g}^{-1}$) in charge and discharge can be determined by the integration of the heat fluxes ($\mu\text{W g}^{-1}$) by the time (h).

The voltage profiles of charge and discharge show a significant capacity loss with increasing current rates, especially in charge cycles. Table S1 summarizes the capacity retention obtained for each C-rate during charge/discharge cycles. As seen in Figure 7, the GCD plateaus can already give significant pointers on the system's behavior at high current densities. At first, the 1.0 C rate shows well-defined cycling plateaus while maintaining an adequate performance (charging and discharging capacity retentions are respectively 87% and 90%). On the other hand, 1.5 C shows less visible charge plateaus next to its discharge counterpart (coming respectively at 17.5% and 85%). Finally, high current rates such as 2 C, 2.5 C, 3 C and 4 C respectively show undefined plateaus and insufficient reversible capacity to further explore their thermal stability.

Heat flux at different current rates were established at different cycling states. The results are given in Table S1 and their evolution is represented as a function of the C-rate in Figure S3. The heat generations are always more important when discharging. Indeed, the kinetic limit of the lithium intercalation is higher than the delithiation limit. This leads to a greater internal resistance during discharge and therefore a greater heat release. The generation of heat in charge is greater than in discharge only during the 1st cycle. This is due to the oxidation of the species present in the electrolyte to form the CEI as explained previously. It is also shown that the heat generation in charge is not affected by the increase in C-rate.

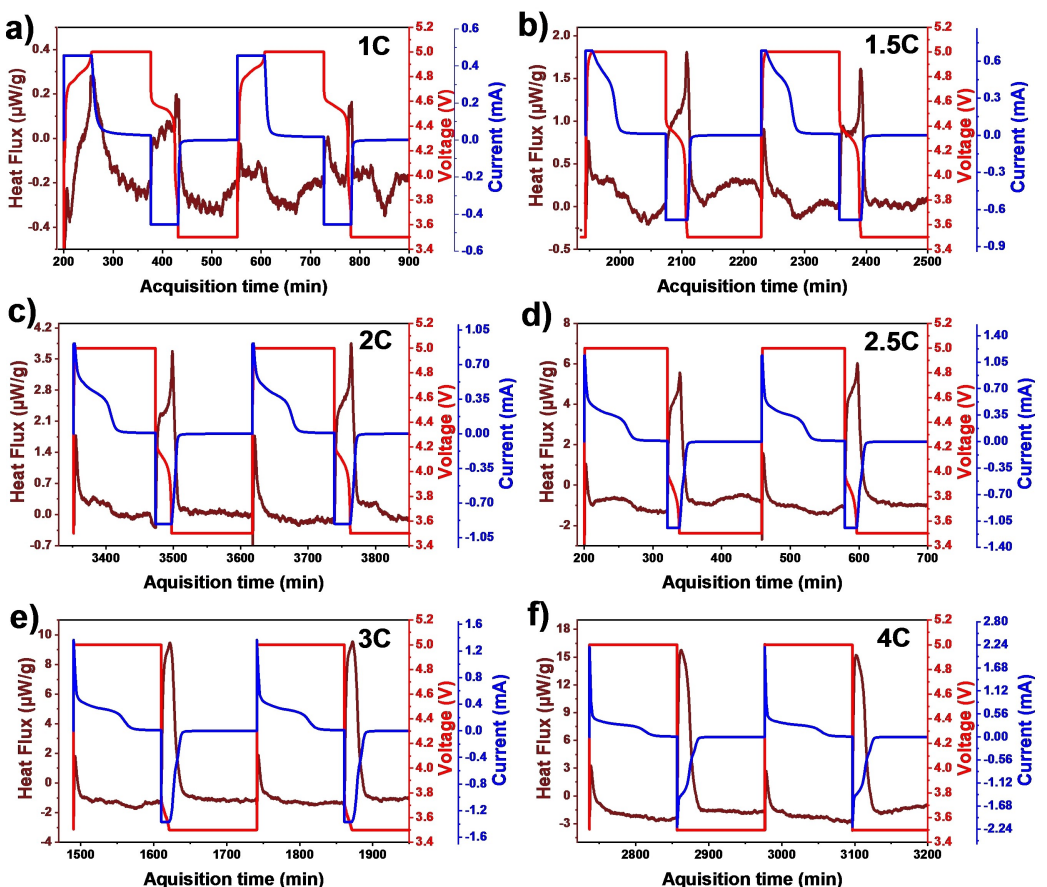


Figure 7. Current, voltage and heat flux profiles of the LMNO | Li half-cell under isothermal mode of 35 °C at a) 1.0 C, b) 1.5 C, c) 2.0 C, d) 2.5 C, e) 3.0 C and f) 4.0 C.

With increasing the C-rates, the exothermic peaks during discharge become more intense and clearer. It is interesting to note that the increase of heat generation is not only due to a Joule effect. Indeed, the coefficient r , given in Table S1 shows that the increase in heat generation is different from that of the current since the value of r is different from that of the C-rate. Considering the abovementioned conclusions, 1.0 C seems to be the best-adapted C-rate for our study since it couples suitable electrochemical performances with well-defined heat flux profiles.

To compare the effect of electrolytes nature on the heat flux profile and internal heat generation of the LMNO | Li half-cell, operando calorimetry measurements were undertaken at 35 °C during cycling at 1.0 C with the 4 prepared electrolytes additive free, FEC, SN and FEC + SN. A floating is applied after each charge at 5.0 V for 2 h. The current, voltage and heat flux profiles obtained are shown in Figure 8(a-d). Regarding the voltage profiles, the charging and discharging plateaus are well defined for all electrolytes additive free, FEC, SN and FEC + SN cells retained respectively 83, 89, 85 and 86.5% of the initial charge capacity after 5 cycles, and 97, 99, 99 and 99% of discharge capacity respectively. Despite the change of additives in the electrolyte, the heat flux profiles overall look similar. The application of current when charging or discharging the battery

induces an increase of the heat fluxes, which decrease during the floating at 5.0 V for the same reasons already explained above. However, electrolyte modification highly impacts the amount of heat generated during cycling. Figure 8(e) exhibits the heat flux profiles of all electrolytes layered with each other. This comparison reveals the significant difference in the heat generated as it presents the integrated area under the heat flux peaks. This area is calculated and represented in Figure 8(f). It is clear that the battery without additive generated the highest amount of heat, with $0.63 \mu\text{Wh g}^{-1}$ and $0.36 \mu\text{Wh g}^{-1}$ during the charge and the discharge respectively. On the contrary, the battery using the FEC/SN mixture generated the lowest heat with only 0.15 and $0.09 \mu\text{Wh g}^{-1}$ for the charge and discharge respectively. Electrolytes based only on FEC or SN generated 0.44 and $0.44 \mu\text{Wh g}^{-1}$ respectively for the charge process and 0.23 and $0.30 \mu\text{Wh g}^{-1}$ respectively for the discharge. The latter values represent 2 to 7 times the heat generated by the FEC + SN electrolyte, indicating the notable effect of the interface modification in improving the thermal stability of a battery. The CEI created would limit the contact between the charged reactive cathode and species present in the electrolyte, thereby reducing the parasitic exothermic reactions and heat generated from the battery, thus improving its thermal safety.

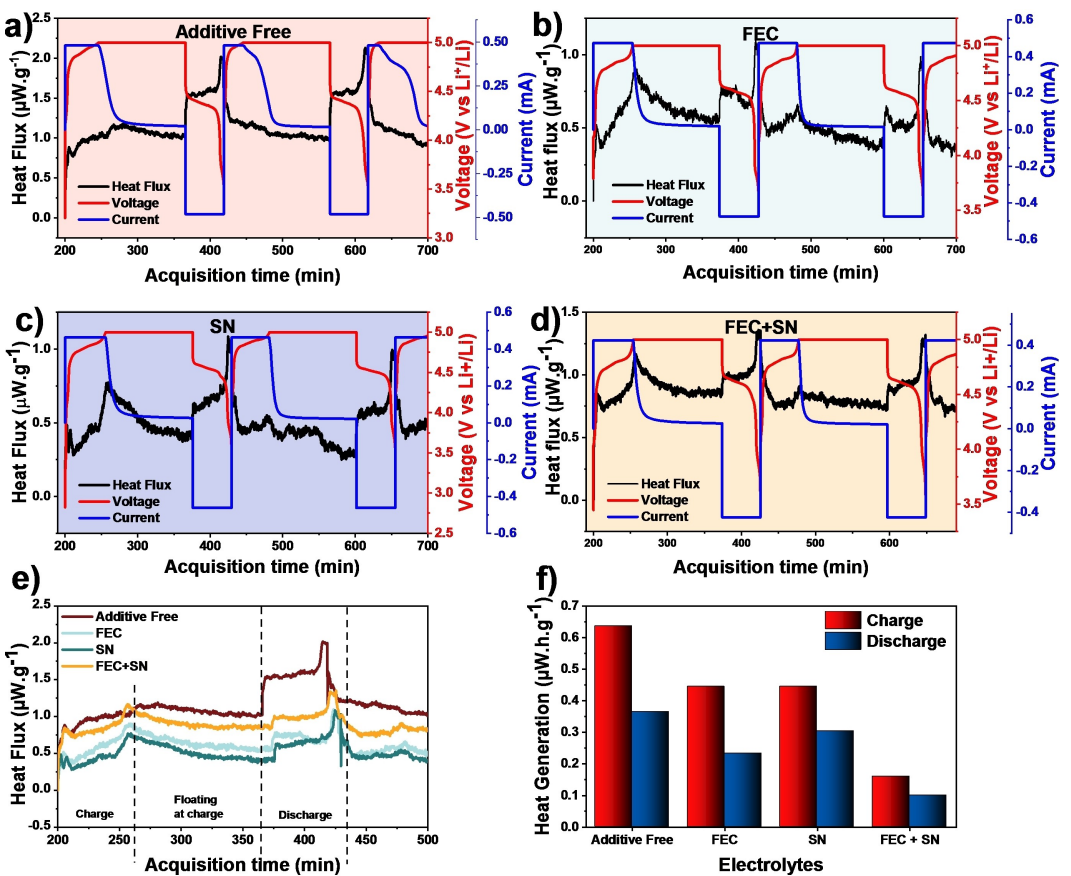


Figure 8. Current, voltage and heat flux profiles of the LMNO|Li half-cell under isothermal mode of 35 °C at 1.0 C with electrolyte a) additive free, b) FEC and c) SN, d) FEC + SN. e) Layered heat flux profiles of the first cycle for all electrolytes. f) Heat generations during charge (red) and discharge (blue) for formulated electrolytes.

More interestingly, we further investigated the heat flux profile of a symmetric Li–Li system to evaluate its contribution in the heat generated by the LMNO–Li battery. Figure S4 exhibits the voltage, current and heat flux profiles of the Li–Li (Figure S4a) and Li–LMNO (Figure S4b) systems of the first cycles under the same scale for an accurate comparison. It is clear that the peaks induced by the plating/stripping processes of the Li–Li cell are distinctly negligible compared to the peaks generated by the charging/discharging of the Li/LMNO battery system. In fact, the Li/LMNO system generated 3.645 and 3.147 μVhcm^{-2} while the Li–Li system only generated 0.829 and 0.404 μVhcm^{-2} after applying a positive and negative current respectively. The LMNO would therefore be the main responsible for the heat generated in the battery, with a minor contribution from lithium metal.

Conclusions

The combination fluoroethylene carbonate (FEC) and succinonitrile (SN) in electrolytes for LMNO–Li batteries resulted in a remarkable improvement of their cycling performance and thermal stability at elevated cut-off voltages. This phenomenon was thoroughly investigated using various electroanalytical

techniques, including linear sweep voltammetry, electrochemical tests and operando calorimetry. The results of these experiments demonstrated that the mixture of 5% FEC with 2% of SN exhibited a wider electrochemical stability window that went from 2.2 without additives to 2.7 V vs. Ag⁺/Ag with FEC + SN. Furthermore, the latter presented superior thermal stability compared to alternative electrolytes. The heat generated by the FEC + SN systems was 7 times less than that generated by the additive free system. The formation of a CEI layer, observed via scanning electron microscopy and confirmed by the electrochemical impedance spectroscopy, was also facilitated using FEC + SN electrolytes, which suppressed the secondary reactions between the electrolyte species and the cathode interface. Electrochemical impedance spectroscopy has shown that the CEI formed by these additives is more conductive in Li⁺. This allows operation of LMNO/Li devices at higher C-rates. This CEI also reduced side reactions between the electrolyte species and LMNO interface, and therefore the amount of heat emitted by these reactions. In conclusion, the utilization of FEC + SN as electrolytes additives confers long-term cycling stability and enhanced safety to lithium-ion batteries, rendering them suitable for use in automotive and grid storage applications.

Materials and Methods

Electrolytes preparation

Studied electrolytes were prepared by dissolving 1.0 mol L⁻¹ of LiPF₆ (purchased from Fluorochem, battery grade) in a mixed solvent of ethylene carbonate (EC) (Sigma-Aldrich) and dimethyl carbonate (DMC) (Sigma-Aldrich) with a weight ratio of 1:1. The addition of 5.0 wt% fluoroethylene carbonate (FEC) (Sigma-Aldrich), 2.0 wt% succinonitrile (SN) (Sigma-Aldrich) or both to the aforementioned reference electrolyte was carried out for the formulation of 4 electrolytes, named respectively additive Free, FEC, SN and FEC + SN. All electrolyte formulations were conducted in an argon filled MBraun glovebox, with less than 10 ppm of moisture. All products used for these formulations have purities greater than 99%. Electrolytes compositions are summarized in the Table 3 below:

Cell assembly and electrochemical tests

The coin cells (CR2032) are composed of a cathode material on aluminum current collector, an electrolyte, a separator (Whatman GF/C) and lithium metal as counter electrode and reference. High voltage positive cathode studied in this work is LiMn_{1.5}Ni_{0.5}O₄ (LMNO). It was purchased from Sigma Aldrich and contain 80% of active material. The electrodes are cut into 10 mm diameter discs, weighed and dried under vacuum at 80 °C for 4 h. The prepared coin cells were assembled in an argon filled glove box with oxygen and moisture content less than 0.1 ppm and 10 ppm respectively.

Electrochemical measurements were carried out at room temperature. The electrolytes oxidation/reduction potentials were evaluated by a Biologic VMP-3 potentiostat using linear sweep voltammetry (LSV) at a scan rate of 5 mVs⁻¹. The electrolyte was sealed in a 3-electrode glass cell. The working and counter electrodes are platinum discs of 7.07 mm² area and the reference electrode is a silver wire.

Electrochemical impedance spectra (EIS) were measured with a VMP-3 potentiostat over the frequency range of 500 kHz to 5 MHz with LiMn_{1.5}Ni_{0.5}O₄ as a cathode and lithium metal as anode.

Galvanostatic cycling and cyclic voltammetry were performed on a Biologic BCS-805 battery cycler or on a Biologic VMP-3 potentiostat between 3.5 V to 5.0 V. All voltages will be referred to the Li/Li⁺ reference couple, unless otherwise stated. All electrochemical tests were systematically reproduced at least 3 times, and therefore the data reported herein are assumed to be representative.

Characterization procedures

Density and viscosity measurements were carried out at atmospheric pressure over a temperature range of 0 to 80 °C with a U-shaped vibrating-tube densimeter (DMA 4500 M, Anton Parr, France) coupled with a rolling-ball microviscosimeter (Lovis 2000 ME, Anton Parr, France). The internal calibration of the densimeter

was confirmed by measuring densities of air and triple-distilled water (25 °C), before every sample measurement, with an accuracy of 1 × 10⁻⁵ g cm⁻³. The optimum angle for the microviscosimeter was automatically determined by the equipment, based on run time. Capillary tubes with nominal internal diameters of 1.59 mm, previously calibrated as a function of temperature and angle of measurements with viscosity standards from the manufacturer, were used for measurements. The viscosity at each temperature was measured 6 times, with an estimated uncertainty of 0.5%.

Electrolytes ionic conductivities were measured using a BioLogic Multichannel Conductivity Meter based on a frequency response analyser (MCM 10) connected to a Peltier temperature-controlled unit with 10 slots (WTS 10). The measurements were carried out in adequate cells with 2 parallel platinum electrodes immersed in the studied electrolytes between -20 and 80 °C. The cells are sealed in the glove box to prevent the samples from exposure to air. The uncertainty of the conductivity measurements was higher than 1 × 10⁻⁴ mS cm⁻¹.

Electrodes were examined by a Zeiss Ultra PLUS field effect scanning electron microscope. Electrodes were collected at a charge state of 5 V and washed in the glovebox using dimethyl carbonate solvent (DMC).

Differential scanning calorimetry (DSC) was performed with a PerkinElmer DSC 4000 for all electrolytes. Samples, initially at 25 °C, were first cooled to -60 °C followed by a 5-minute isothermal plateau at this temperature, then heated up to 250 °C. Each scan was performed at 5 °C min⁻¹. The DSC pans were sealed inside the glove box to prevent electrolytes from exposure to air.

The DSC was also used with LMNO electrodes charged at 5 V. The batteries were disassembled in a glove box in order to recover the charged active material and seal it in the DSC pans. Same experiment parameters as for electrolytes were carried out.

Operando accelerating rate calorimetry test (ARC)

The operando profiles of the heat fluxes from LMNO|Li half-cells are obtained with a multimode calorimeter (Netzsch, MMC 274 Nexus, Germany). These measurements were conducted in coin cells placed directly in the calorimeter connected to an electrochemical cycler (SP-50 Bio-Logic, France) to adjust the desired currents and potentials. This device operates similarly to the Differential Scanning Calorimeter (DSC) and includes a reference cell and a sample cell. A coin cell filled with argon is used as a reference. The total heat generation of each step can be obtained by integrating the heat flux curve. The isothermal mode was selected in this work, with a temperature of 35 °C. Each cell was cycled 5 times in a voltage range from 3.5 V to 5.0 V (vs. Li/Li⁺).

Acknowledgements

The authors would like to thank the Mohammed VI Polytechnic University, Tours University and the PHC-Toubkal N° TBK/20/108-CAMPUS N°41673NF program for financial support to the researchers involved in this study.

Conflict of Interests

The authors declare no conflict of interest.

Table 3. Electrolytes compositions.

Code	Composition*
AF	1 M LiPF ₆ in 1:1 wt.% EC:DMC
FEC	AF + FEC 5 wt.%
SN	AF + SN 2 wt.%
FEC + SN	AF + FEC 5 wt.% + SN 2 wt.%

*EC = ethylene carbonate, DMC = dimethyl carbonate, AF = additive free, FEC = fluoroethylene carbonate, SN = succinonitrile.

Data Availability Statement

The data that support the findings of this study are available from the corresponding author upon reasonable request.

Keywords: additives · CEI · electrolyte · high voltage cathode · lithium-ion batteries

- [1] M. Li, J. Lu, Z. Chen, K. Amine, *Adv. Mater.* **2018**, *30*, 1800561.
[2] J. Xiang, Y. Wei, Y. Zhong, Y. Yang, H. Cheng, L. Yuan, H. Xu, Y. Huang, *Adv. Mater.* **2022**, *34*, 2200912.
[3] A. Kraytsberg, Y. Ein-Eli, A. Kraytsberg, Y. Ein-Eli, *Adv. Energy Mater.* **2012**, *2*, 922–939.
[4] W. Li, B. Song, A. Manthiram, *Chem. Soc. Rev.* **2017**, *46*, 3006–3059.
[5] N. Tolganbek, Y. Yerkinbekova, S. Kalybekkazy, Z. Bakenov, A. Mentbayeva, *J. Alloys Compd.* **2021**, *882*, 160774.
[6] M. Baazizi, M. Dahbi, M. Aqil, F. Ghamouss, I. Saadoune, *2019 7th Int. Renew. Sustain. Energy Conf. IRSEC*, IEEE, **2019**, 2019.
[7] W. Zhao, J. Zheng, L. Zou, H. Jia, B. Liu, H. Wang, M. H. Engelhard, C. Wang, W. Xu, Y. Yang, J. G. Zhang, *Adv. Energy Mater.* **2018**, *8*, 1800297.
[8] Y. Xia, J. Zheng, C. Wang, M. Gu, *Nano Energy* **2018**, *49*, 434–452.
[9] G. Liang, V. K. Peterson, K. W. See, Z. Guo, W. K. Pang, *J. Mater. Chem. A* **2020**, *8*, 15373–15398.
[10] J. H. Kim, N. P. W. Pieczonka, L. Yang, *ChemPhysChem* **2014**, *15*, 1940–1954.
[11] S. Sayah, M. Baazizi, M. Karbak, J. Jacquemin, F. Ghamouss, *Energy Technol.* **2023**, 2201446.
[12] S. S. Zhang, *Energy Storage Mater.* **2020**, *24*, 247–254.
[13] T. Li, X. Z. Yuan, L. Zhang, D. Song, K. Shi, C. Bock, *Electrochem. Energy Rev.* **2019**, *31*, 43–80.
[14] X. M. Fan, Y. De Huang, H. X. Wei, L. B. Tang, Z. J. He, C. Yan, J. Mao, K. H. Dai, J. C. Zheng, *Adv. Funct. Mater.* **2022**, *32*, 2109421.
[15] Y. Lei, J. Ni, Z. Hu, Z. Wang, F. Gui, B. Li, P. Ming, C. Zhang, Y. Elias, D. Aurbach, Q. Xiao, *Adv. Energy Mater.* **2020**, *10*, 2002506.
[16] L. J. Fu, H. Liu, C. Li, Y. P. Wu, E. Rahm, R. Holze, H. Q. Wu, *Solid State Sci.* **2006**, *8*, 113–128.
[17] Y. Cheng, Y. Sun, C. Chu, L. Chang, Z. Wang, D. Zhang, W. Liu, Z. Zhuang, L. Wang, *Nano Res.* **2022**, *15*, 4091–4099.
[18] T. F. Yi, J. Mei, Y. R. Zhu, *J. Power Sources* **2016**, *316*, 85–105.
[19] H. Qian, H. Ren, Y. Zhang, X. He, W. Li, J. Wang, J. Hu, H. Yang, H. M. K. Sari, Y. Chen, X. Li, *Electrochem. Energy Rev.* **2022**, *54*, 1–32.
[20] G. Liang, Z. Wu, C. Didier, W. Zhang, J. Cuan, B. Li, K.-Y. Ko, P.-Y. Hung, C.-Z. Lu, Y. Chen, G. Leniec, S. M. Kaczmarek, B. Johannessen, L. Thomsen, V. K. Peterson, W. K. Pang, Z. Guo, *Angew. Chemie* **2020**, *132*, 10681–10689.
[21] K. Guo, S. Qi, H. Wang, J. Huang, M. Wu, Y. Yang, X. Li, Y. Ren, J. Ma, *Small Sci.* **2022**, *2*, 2100107.
[22] W. Zhang, Q. Ma, X. Liu, S. Yang, F. Yu, *RSC Adv.* **2021**, *11*, 15091–15098.
[23] A. Tsurumaki, M. Agostini, R. Poiana, L. Lombardo, E. Lufrano, C. Simari, A. Matic, I. Nicotera, S. Panero, M. A. Navarra, *Electrochim. Acta* **2019**, *316*, 1–7.
[24] H. Niu, L. Wang, P. Guan, N. Zhang, C. Yan, M. Ding, X. Guo, T. Huang, X. Hu, *J. Energy Storage* **2021**, *40*, 102659.
[25] W. Wu, Y. Bai, X. Wang, C. Wu, *Chinese Chem. Lett.* **2021**, *32*, 1309–1315.
[26] H. Zhi, L. Xing, X. Zheng, K. Xu, W. Li, *J. Phys. Chem. Lett.* **2017**, *8*, 6048–6052.
[27] Z. Hu, F. Xian, Z. Guo, C. Lu, X. Du, X. Cheng, S. Zhang, S. Dong, G. Cui, L. Chen, *Chem. Mater.* **2020**, *32*, 3405–3413.
[28] L. Hu, Z. Zhang, K. Amine, *Electrochim. Commun.* **2013**, *35*, 76–79.
[29] S. L. Glazier, L. E. Downie, J. Xia, A. J. Louli, J. R. Dahn, *J. Electrochem. Soc.* **2016**, *163*, A2131.
[30] R. Narayan, R. Dominko, *Nat. Rev. Chem.* **2022**, *6*, 449–450.
[31] X. Q. Zhang, X. B. Cheng, X. Chen, C. Yan, Q. Zhang, *Adv. Funct. Mater.* **2017**, *27*, 1605989.
[32] C. Xu, F. Lindgren, B. Philippe, M. Gorgoi, F. Björrefors, K. Edström, T. Gustafsson, *Chem. Mater.* **2015**, *27*, 2591–2599.
[33] K. Schroder, J. Alvarado, T. A. Yersak, J. Li, N. Dudney, L. J. Webb, Y. S. Meng, K. J. Stevenson, *Chem. Mater.* **2015**, *27*, 5531–5542.
[34] E. Markevich, G. Salitra, K. Fridman, R. Sharabi, G. Gershinsky, A. Garsuch, G. Semrau, M. A. Schmidt, D. Aurbach, *Langmuir* **2014**, *30*, 7414–7424.
[35] A. Bordes, K. S. Eom, T. F. Fuller, *J. Power Sources* **2014**, *257*, 163–169.
[36] Y. S. Kim, T. H. Kim, H. Lee, H. K. Song, *Energy Environ. Sci.* **2011**, *4*, 4038–4045.
[37] G.-Y. Kim, R. Petibon, J. R. Dahn, *J. Electrochem. Soc.* **2014**, *161*, A506–A512.
[38] Q. Zhang, K. Liu, F. Ding, W. Li, X. Liu, J. Zhang, *Electrochim. Acta* **2019**, *298*, 818–826.
[39] R. Chen, F. Liu, Y. Chen, Y. Ye, Y. Huang, F. Wu, L. Li, *J. Power Sources* **2016**, *306*, 70–77.
[40] Z. Zhu, Y. Tang, Z. Lv, J. Wei, Y. Zhang, R. Wang, W. Zhang, H. Xia, M. Ge, X. Chen, *Angew. Chem.* **2018**, *130*, 3718–3722.
[41] Y. Park, S. H. Shin, H. Hwang, S. M. Lee, S. P. Kim, H. C. Choi, Y. M. Jung, *J. Mol. Struct.* **2014**, *1069*, 157–163.
[42] D. Liu, K. Qian, Y.-B. He, D. Luo, H. Li, M. Wu, F. Kang, B. Li, *Electrochim. Acta* **2018**, *269*, 378–387.
[43] Y. Xu, J. Liu, L. Zhou, L. Zeng, Z. Yang, *J. Electroanal. Chem.* **2017**, *791*, 109–116.
[44] J. Xia, M. Nie, J. C. Burns, A. Xiao, W. M. Lamanna, J. R. Dahn, *J. Power Sources* **2016**, *307*, 340–350.
[45] J. Im, J. Lee, M.-H. Ryou, Y. M. Lee, K. Y. Cho, *J. Electrochem. Soc.* **2017**, *164*, A6381.
[46] L. Wang, Y. Ma, Y. Qu, X. Cheng, P. Zuo, C. Du, Y. Gao, G. Yin, *Electrochim. Acta* **2016**, *191*, 8–15.
[47] J. Bi, D. Mu, B. Wu, J. Fu, H. Yang, G. Mu, L. Zhang, F. Wu, *J. Mater. Chem. A* **2020**, *8*, 706–713.
[48] X. L. Wu, S. Xin, H. H. Seo, J. Kim, Y. G. Guo, J. S. Lee, *Solid State Ionics* **2011**, *186*, 1–6.
[49] L. Z. Fan, Y. S. Hu, A. J. Bhattacharyya, J. Maier, *Adv. Funct. Mater.* **2007**, *17*, 2800–2807.
[50] C. Ho, I. D. Raistrick, R. A. Huggins, *J. Electrochem. Soc.* **1980**, *127*, 343–350.
[51] C. Liang, L. Jiang, Q. Wang, J. Sun, *Fire Techn.* **2020**, 2387–2404.
[52] T. Wu, H. Chen, Q. Wang, J. Sun, *J. Hazard. Mater.* **2018**, *344*, 733–741.
[53] D. Bernardi, E. Pawlikowski, J. Newman, *Electrochim. Soc. Ext. Abstr.* **1984**, *84–2*, 164–165.

Manuscript received: April 10, 2023

Revised manuscript received: June 23, 2023

Accepted manuscript online: June 25, 2023

Version of record online: July 17, 2023